Floquet engineering in the presence of optically excited carriers

Mitchell A. Conway,[1,2] Jonathan O. Tollerud,[1,2] Thi-Hai-Yen Vu,[3,4] Kenji Watanabe [ORCID],[5] Takashi Taniguchi,[6] Michael S. Fuhrer,[3,4] Mark T. Edmonds,[3,4,7] and Jeffrey A. Davis [ORCID][1,2,*]

[1]*Optical Sciences Centre, Swinburne University of Technology, Hawthorn, 3122, Victoria, Australia*

[2]*ARC Centre of Excellence in Future Low-Energy Electronics Technologies, Swinburne University of Technology, Hawthorn, 3122, Victoria, Australia*

[3]*ARC Centre of Excellence in Future Low-Energy Electronics Technology, Monash University, Clayton, 3800, Victoria, Australia*

[4]*School of Physics and Astronomy, Monash University, Clayton, 3800, Victoria, Australia*

[5]*Research Center for Electronic and Optical Materials, National Institute for Materials Science, 1-1 Namiki, Tsukuba 305-0044, Japan*

[6]*Research Center for Materials Nanoarchitectonics, National Institute for Materials Science, 1-1 Namiki, Tsukuba 305-0044, Japan*

[7]*ANFF-VIC Technology Fellow, Melbourne Centre for Nanofabrication, Victorian Node of the Australian National Fabrication Facility, Clayton, VIC 3168, Australia*

Floquet engineering provides an optical means to manipulate electronic bandstructures, however, carriers excited by the pump field can lead to an effective heating, and can obscure measurement of the band changes. Here, we use multidimensional coherent spectroscopy to create a coherent ensemble of excitons in monolayer WS$_2$ and measure the evolution of the coherence throughout the duration of the Floquet pump pulses with constant fluence but varying pulse duration. Changes to the amplitude of the macroscopic coherence quantifies the additional broadening introduced by interactions with carriers excited via two-photon absorption of the red-detuned pump. At the same time, the evolution of the average phase allows the instantaneous changes to the bandstructure to be quantified, which is demonstrated to be independent of the additional broadening. This approach to measuring the evolution of Floquet-Bloch states demonstrates a means to quantify effective heating and nonadiabaticity caused by excited carriers, while at the same time resolving the coherent evolution of the bandstructure.

I. INTRODUCTION

Floquet theory [1] describes the modification of state energies, and in condensed matter the bandstructure, by a periodic perturbation. Coherent light-matter interactions, for example, lead to the formation of photon-dressed band replicas (Floquet-Bloch bands) [2,3], and can enable transient control of bandgap energies via an AC-Stark effect [4,5] or produce exotic nonequilibrium electronic states [6,7]. For example, interacting Floquet-Bloch states have been demonstrated to facilitate a topological phase transition in graphene [8]. Similar effects have been predicted to arise in monolayer transition metal dichalcogenides (TMDCs) [5,9], however, observations of a topological phase transition in these systems remain elusive. This is partially due to the challenges associated with disentangling light-induced bandstructure changes from photoexcited population effects. Furthermore, understanding the role of excited carriers and the resultant heating in the Floquet bandstructure is a key challenge to realizing practical applications of Floquet engineering [10–12].

There have been numerous reports of monolayer TMDCs driven by a red-detuned Floquet pump pulse that use transient absorption measurements to show changes to the bandgap induced by the AC-Stark effect [4–6,13–19]. Recently, the effects of Floquet engineering on a coherent ensemble of excitons was investigated in monolayer tungsten disulphide (WS$_2$) using multidimensional coherent spectroscopy (MDCS) [20]. The coherent ensemble proved particularly sensitive to nonadiabatic effects, revealing an effective power broadening phenomenon at high pump fluences. This broadening occurred only during the pump pulse, and was attributed to interactions between the virtual excitations created by the below resonance Floquet driving field and the excitons in the coherent ensemble. Despite these interactions and resultant broadening, the heterodyne detected signal phase smoothly followed the dynamics of the pump envelope. Whilst no incoherent photocarriers were created by the pump, that work suggested the average signal phase measured is not impacted by losses in the macroscopic coherence of the ensemble. This picture is consistent with previous theoretical work demonstrating that Floquet effects are present despite dissipation [21], which suitably described a Floquet-topological phase transition in graphene [8]. The impact of real photocarriers on Floquet effects in semiconductor systems has not previously been precisely quantified. Here we demonstrate that MDCS can reliably separate changes to the bandstructure from broadening caused by excited carriers, an important demonstration in the pursuit of realizing a Floquet-topological phase transition in monolayer TMDCs.
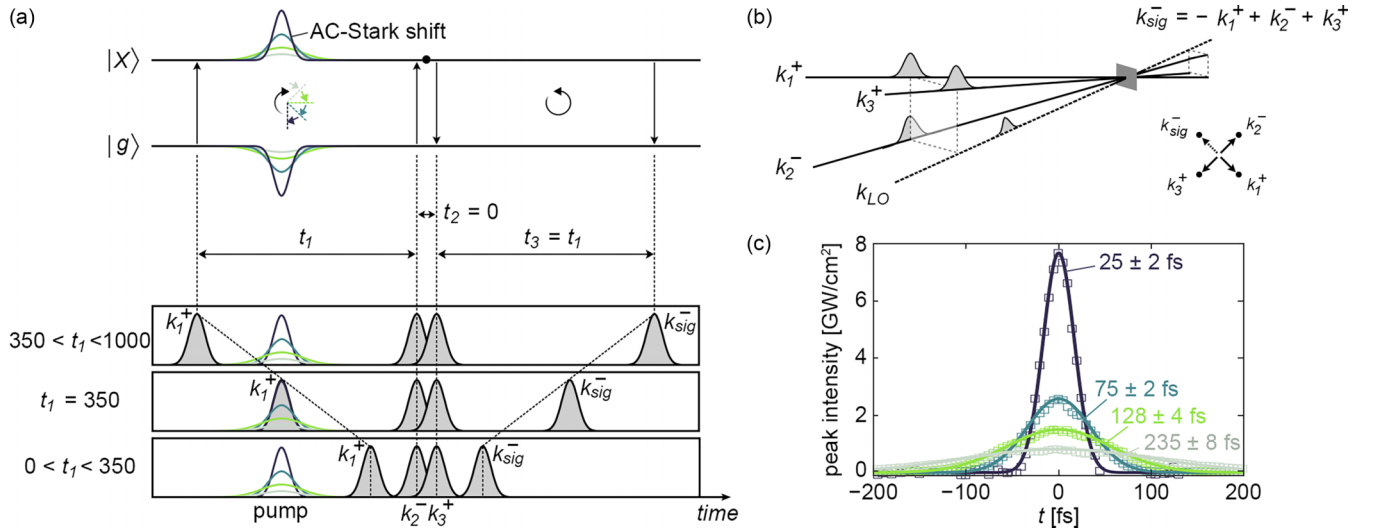
*JDavis@swin.edu.au

104302-1

FIG. 1. (a) Schematic representation of our pumped 1Q-MDCS measurements. The arrival of the first excitation pulse $\mathbf{k}_1^+$ creates a coherent superposition between the ground state $|g\rangle$ and the K' valley exciton state, $|X\rangle$. This 1Q coherence evolves during the first interpulse delay t_1. Following the same approach used in Ref. [20], we introduce a red-detuned σ^+ polarized pump pulse arriving ~350 fs before $\mathbf{k}_2^-$ and $\mathbf{k}_3^+$, indicated by the colored Gaussian pulses. As a result, the phase of the $|g\rangle\langle X|$ coherence excited by $\mathbf{k}_1^+$ oscillates faster while the pump is present due to an AC-Stark shift of the $|g\rangle$ and $|X\rangle$ state energies, which induces additional phase rotation of the measured signal. As the pump is stationary in time while $\mathbf{k}_1^+$ is scanned, three different pulse orderings occur: in the interpulse delay range $0 < t_1 < 350$ fs, $\mathbf{k}_1^+$ arrives after the pump; at $t_1 = 350$ fs the pump and $\mathbf{k}_1^+$ overlap in time; and for $350 < t_1 < 1000$ fs, $\mathbf{k}_1^+$ arrives before the pump. The coherence $|g\rangle\langle X|$ evolves until the simultaneous arrival of pulses $\mathbf{k}_2^-$ and $\mathbf{k}_3^+$. After the three excitation pulses interact with the sample, a third-order polarization is generated which radiates as the four-wave mixing signal, with wave vector $\mathbf{k}_{sig}^- = -\mathbf{k}_1^+ + \mathbf{k}_2^- + \mathbf{k}_3^+$. The four beam box geometry utilized in our experiments is depicted in (b). (c) Temporal profiles of the pump pulses acquired from the deconvolution of a cross correlation between the pump and $\mathbf{k}_1^+$ beam. Throughout this work, we utilize four different pump beams which are 25, 75, 128, and 235 fs in duration with corresponding peak intensities of 7.7, 2.6, 1.5, and 0.8 GW/cm^2, respectively. All pump beams have the same total fluence of 205 μJ/cm^2, and are centered at 1.82 eV (red shifted from the A-exciton resonance by ~260 meV).

Here we perform MDCS measurements with an additional red-detuned pump pulse to drive an AC-Stark shift, but vary the pump duration, while keeping the total fluence the same. We find that as the duration of the pump pulses is decreased, the corresponding increase in the peak intensity introduces additional carriers via two-photon absorption. In this regime, Floquet engineering effects are convolved with incoherent carrier injection which acts to obscure signatures of the band-structure changes. In particular, these additional carriers lead to increased scattering and decoherence, which we are able to quantify. However, despite these losses in macroscopic co-herence, we find that the evolution of the phase of the MDCS signal, which follows the average phase of the excitonic coher-ent superposition, is not impacted. From this phase evolution we are able to extract changes to the bandstructure, even in the presence of substantial photoexcited populations.

II. EXPERIMENTAL METHODS

In our MDCS measurements, three light-matter interac-tions trigger a third-order sample response, which is measured as a function of the interpulse delays [22]. In one-quantum MDCS measurements (1Q-MDCS), the arrival of the first excitation pulse $\mathbf{k}_1^+$ (with wave vector $\mathbf{k}_1$ and the "+" indicat-ing σ^+ circular polarization) creates a coherent superposition between the ground state and the K' exciton state. The state of the system in this time period is described by the density oper-ator, $|g\rangle\langle X_{K'}|$. With g and $X_{K'}$ being eigenstates of the system,

only one term is nonzero: the one that quantifies the coherence between g and $X_{K'}$ [20,22–24]. This 1Q coherence evolves during the first interpulse delay, t_1, where the evolution of $|g\rangle\langle X_{K'}|$ is proportional to $\exp[(-i\omega_{K'}t_1)]$, and is measured by scanning the arrival time of $\mathbf{k}_1^+$. The simultaneous arrival of the final two excitation pulses, with wave vectors $\mathbf{k}_2$ and $\mathbf{k}_3$ and circular polarization σ^- and σ^+, respectively, generates a third-order polarization ($|X_K\rangle\langle g|$) which radiates as the four-wave mixing signal in the direction given by $\mathbf{k}_{sig}^- = -\mathbf{k}_1^+ + \mathbf{k}_2^- + \mathbf{k}_3^+$. The four-wave mixing signal is overlapped with a reference pulse ($\mathbf{k}_{LO}^-$) for heterodyne detection, and spectrally resolved to give the amplitude and phase of the signal as a function of the emission energy, $\hbar\omega_3$. A schematic representa-tion of the MDCS pulse ordering and four beam box geometry utilized in our measurements is depicted in Figs. 1(a) and 1(b), respectively. The MDCS excitation pulses were 30 ± 1 fs in duration, with a fluence of 1.2 ± 0.2 μJ/cm^2, and focused to a 36 ± 5 μm spot at the sample surface (see the Supplemental Material for the spectrum of the MDCS pulses [25]).

To measure an AC-Stark effect in monolayer WS$_2$, we employed the same technique outlined in Ref. [20]. The σ^+ polarized pump was red detuned by ~260 meV from the low temperature A-exciton energy of 2.087 eV, and set to arrive 350 fs before $\mathbf{k}_2^-$ and $\mathbf{k}_3^+$. To control the pump du-ration, we utilized a pulse shaper based around a spatial-light modulator [26], which enabled control of the spectral phase and amplitude of our pulses. The pulse shaper was first used to ensure a flat spectral phase across the pump pulse using
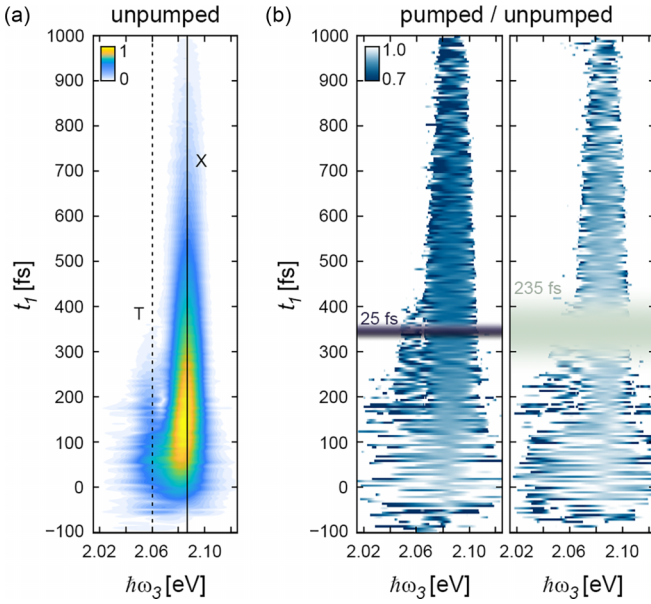
FIG. 2. (a) Normalized 1Q-MDCS signal amplitude as a function of t_1 and $\hbar\omega_3$ (emission energy) in the absence of the pump. Two peaks at $\hbar\omega_3 = 2.086$ and $\hbar\omega_3 = 2.060$ eV are attributed to the A-exciton and trion peak, respectively. (b) Ratio of pumped and unpumped 1Q-MDCS signal amplitude for a pump duration of 25 $\pm$ 2 and 235 $\pm$ 8 fs. The blue feature indicates that the amplitude is reduced by the pump, and this loss in macroscopic coherence is greater for a shorter pump duration (despite the same pump fluence of 205 μJ/cm^2). This loss in macroscopic coherence is due to an increase in exciton-free carrier interactions created by two-photon absorption of the pump.

the multiphoton intrapulse interference phase scan technique [27]. This yielded a 25 $\pm$ 2 fs duration for the full spectral bandwidth of the pump pulse output from a noncolinear optical parametric amplifier (see the Supplemental Material [25] for pump spectrum). To increase the pulse duration, the spectral bandwidth was reduced by the pulse shaper, while maintaining a flat spectral phase. This has the consequence of reducing the pump fluence, so to ensure the total integrated energy of the pump pulse was constant, a variable neutral density filter was used to control the intensity. The measurements for all pulse durations were conducted with pump fluence of 205 $\pm$ 10 μJ/cm^2 with a pump spot size of 67 $\pm$ 5 μm at the sample surface. Figure 1(b) shows the temporal profile for each of the pump pulses utilized in this work, measured by deconvolving the cross correlation of the pump and the $\mathbf{k}_1^+$ excitation beam.

III. RESULTS AND DISCUSSION

A. Quantifying loss of macroscopic coherence due to two-photon absorption

Figure 2(a) shows the 1Q signal amplitude as a function of t_1 and $\hbar\omega_3$, in the absence of the pump. Two peaks at $\hbar\omega_3 = 2.087$ and $\hbar\omega_3 = 2.060$ eV are evident and attributed to the A-exciton and trion peak, respectively [20,23]. The exciton and trion energies are blue shifted by ~15 meV from the equivalent peaks in Ref. [20], which arises from the differ-

ence in samples. In Ref. [20], the WS$_2$ monolayer was fully encapsulated in hexagonal-Boron Nitride (hBN), while the sample used in this work has only a bottom hBN layer (see the Supplemental Material [25] for sample characterization). The unpumped signal amplitude decays as a function of t_1 due to decoherence of $|g\rangle\langle X_{K'}|$, with a decoherence time of 430 ± 10 fs, consistent with previous MDCS measurements of excitons in monolayer TMDCs [20,23,24,28].

Figure 2(b) shows the ratio of the signal amplitude with the pump on (pumped) and the signal amplitude with the pump off (unpumped), for pump pulses 25 ± 2 fs and a 235 ± 8 fs in duration arriving 350 fs before $\mathbf{k}_2^-$ and $\mathbf{k}_3^+$ [shaded regions in Fig. 2(b)]. These plots show a decrease in the signal amplitude with the introduction of the σ^+ polarized pump, due to additional decoherence of $|g\rangle\langle X_{K'}|$. The decrease in amplitude and loss in macroscopic coherence becomes more significant for the shorter pump pulse with higher peak intensity.

To more clearly see the dynamics of the decay and additional decoherence induced by the pump pulse, we integrate the ratio of the pumped and unpumped signal amplitudes around the exciton emission energy ($\hbar\omega_3 = 2.087 \pm 0.009$ eV), as shown in Fig. 3(a). A ratio of one indicates the amplitude of the signal with the pump on and off are the same, whilst ratios below one indicate the pump is inducing additional decoherence and decay of the signal amplitude. For $0 < t_1 < 350$ fs, the pump arrives before $\mathbf{k}_1^+$ and during this period the ratio of signal amplitudes is decreasing. For $t_1 > 350$ fs the ratio remains roughly constant, indicating no further additional decoherence is present. This behavior is consistent with extra carriers being created by the pump pulse and remaining for the duration of the experiment: For $0 < t_1 < 350$ fs the $|g\rangle\langle X_{K'}|$ coherence evolves in the presence of the extra carriers created by the pump, leading to additional scattering and decoherence. For $t_1 > 350$ fs, $\mathbf{k}_1^+$ arrives before the pump and the $|g\rangle\langle X_{K'}|$ coherence is not affected by the extra carriers until the pump arrives, 350 fs before $\mathbf{k}_2^-$ and $\mathbf{k}_3^+$. In this case, the period when there is additional scattering and decoherence is fixed, and so the ratio of pumped to unpumped signal amplitude does not change.

To quantify the additional coherence we need to take into account that the signal decay is not exponential over this time period, due to a combination of photon echo and free-induction decay. In this case the signal amplitude integrated as a function of $\hbar\omega_3$ is given by [29,30]

$$S = \frac{e^{\frac{1}{2}\gamma(\frac{\gamma}{\sigma^2} - 4t_1)}\sqrt{\frac{\pi}{2}}\mathrm{erfc}\left[\frac{\gamma - \sigma^2 t_1}{\sqrt{2}\sigma}\right]}{\sigma}, \tag{1}$$

where γ is the unpumped homogeneous linewidth, σ is the inhomogeneous linewidth, and erfc is the complementary error function. Inset into Fig. 3(a) is the unpumped data (black points), which was fit by Eq. (1) (red line) to determine the values for $\gamma = 1.45 \pm 0.08$ meV and $\sigma = 7.4 \pm 0.9$ meV.

To quantify the additional decoherence when the pump was introduced, we assumed that the decoherence rate for $0 < t_1 < 350$ fs was increased and constant for a given pulse duration.
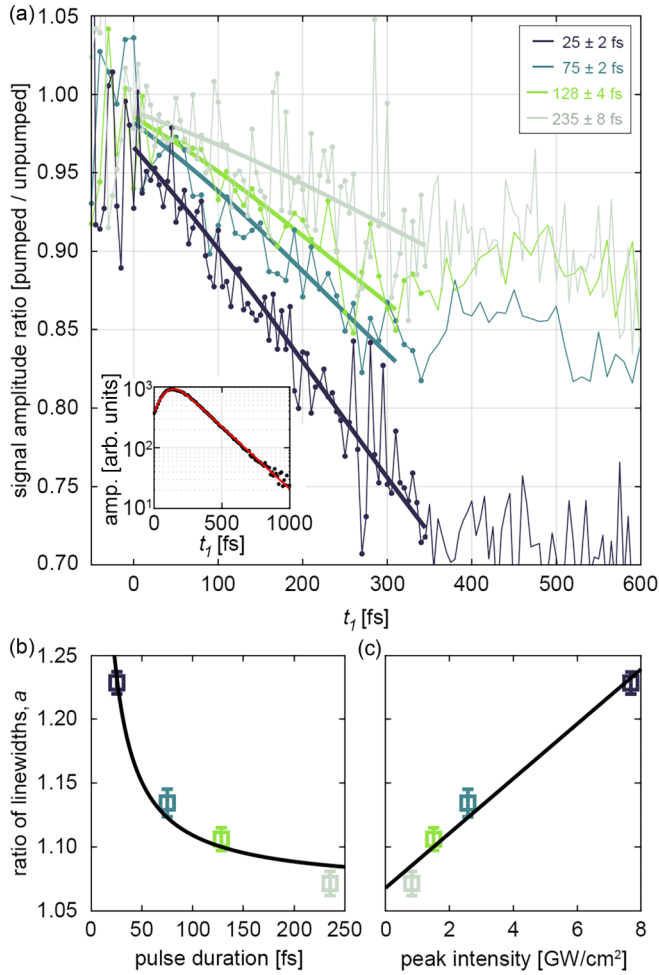
FIG. 3. (a) Ratio of the pumped to unpumped signal amplitude (i.e., slices through Fig. 2(b) at the exciton emission energy) fit by Eq. (2) (solid lines) for each pump pulse duration. Inset: unpumped signal amplitude as a function of t_1 (black points) was fit with Eq. (1) (red line) to determine the values for $\gamma = 1.45 \pm 0.08$ meV and $\sigma = 7.4 \pm 0.9$ meV. (b) and (c) show the values for a, the ratio of the homogeneous linewidths for the pump on and off, plotted as a function of pulse duration and peak intensity, respectively.

The ratio of pumped and unpumped data is then given by

$$\frac{S_{\text{on}}}{S_{\text{off}}} = \frac{e^{\frac{1}{2}a\gamma\left(\frac{a\gamma}{\sigma^2} - 4t_1\right)}\sqrt{\frac{\pi}{2}}\text{erfc}[\frac{a\gamma - \sigma^2 t_1}{\sqrt{2}\sigma}]}{e^{\frac{1}{2}\gamma\left(\frac{\gamma}{\sigma^2} - 4t_1\right)}\sqrt{\frac{\pi}{2}}\text{erfc}[\frac{\gamma - \sigma^2 t_1}{\sqrt{2}\sigma}]}, \qquad (2)$$

where a is the ratio of the homogeneous linewidths for the pump on and off. With a being the only fit parameter, Eq. (2) fit very well to the data shown in Fig. 3(a) to determine the increase in homogeneous linewidth, or equivalently, decoherence rate. The values for a are plotted as a function of pulse duration and peak intensity in Figs. 3(b) and 3(c), respectively. Additional decoherence due to scattering from photoexcited carriers would be expected to vary linearly with the density of carriers and thus linearly with the total fluence [22]. With constant fluence, the linear increase is indicative of a process that varies quadratically with intensity, such as two-photon absorption. Briefly, this can be understood as

follows: The total number of two-photon events is proportional to $\int_{-\infty}^{\infty} I(t)^2 dt$, where $I(t)$ is the intensity profile of the pump pulse given by $I(t) = \frac{1}{\delta\sqrt{2\pi}}\exp(\frac{-t^2}{2\delta^2})$, with the pulse duration given by the full width at half maximum, FWHM $= 2\sqrt{2\ln 2}\,\delta$, and the peak intensity by $\frac{1}{\delta\sqrt{2\pi}}$. Rearranging this integral gives $\frac{1}{\delta\sqrt{2\pi}}\int_{-\infty}^{\infty}\frac{1}{\sqrt{2}}I(t)dt$. With constant pump fluence [i.e., $\int_{-\infty}^{\infty} I(t)dt$ is constant], the number of two-photon events is then linearly proportional to the peak intensity (or the inverse of the pulse duration).

The additional decoherence when the pump is on is therefore attributed to scattering with carriers excited by two-photon absorption. We expect these excited carriers to remain in the system, though likely not in the same state, for several ps or longer [31–35], well beyond the timescale of our measurements. In order to estimate the carrier density, we compare the change of the decoherence time/homogeneous linewidth to resonant measurements that show the homogeneous linewidth dependence on exciton density, as shown in the Supplemental Material [25]. Assuming the interaction strength of the two-photon excited carriers is similar to that of the A exciton (0.1015×10^{-10} meV $\cdot$ cm^2), we estimate that for the shortest pulses, and a measured increase in γ of 0.33 meV (from 1.45 meV to 1.78 meV), the carrier density created by the Floquet pump pulse was 3.3×10^{10} cm^{-2}. With the pump red shifted from the exciton transition by $\sim$260 meV, and centered at 1.82 eV, the precise identification of states available beyond 3.6 eV is challenging as it includes a multitude of high energy conduction bands in monolayer WS$_2$, and transitions beyond the K points in the Brillouin zone. As a rigorous treatment is outside the scope of this work, we consider the two-photon absorption of the red-detuned pump capable of accessing continuum states which enables the creation of free carriers.

The two-photon absorption and accelerated decoherence for $0 < t_1 < 350$ observed here was not evident in the previous measurements of Ref. [20]. In comparison, the highest pump peak intensity used here was 7.7 ± 0.4 GW/cm^2 for the 25 fs pump pulse duration, which is similar to the highest peak intensity reached in Ref. [20], 7.1 ± 0.5 GW/cm^2, where two-photon absorption was not evident. The reason is not entirely understood, however, it is possible that the differences come from the different encapsulation environments of the samples used. The impact of top-layer hBN encapsulation on two-photon absorption in monolayer TMDCs has not been well studied. Additionally, different degrees of aging and defects [36–38] may influence two-photon processes. These questions are left for future work.

B. Identifying bandstructure changes using the signal phase

Figure 4(a) shows the evolution of the difference (pumped minus unpumped) of the measured signal phase as a function of t_1, averaged over the exciton energy ($\hbar\omega_3 = 2.087 \pm 0.009$ eV). For the first 200 fs there is no phase shift, until $\mathbf{k}_1^+$ begins to overlap with the pump pulse. The pump, through the AC-Stark effect, blue shifts the K' exciton, which causes the phase of the $|g\rangle\langle X_{K'}|$ coherence (and hence the signal) to evolve faster. The rate at which the phase shift evolves is determined by the magnitude of the blue shift, which is
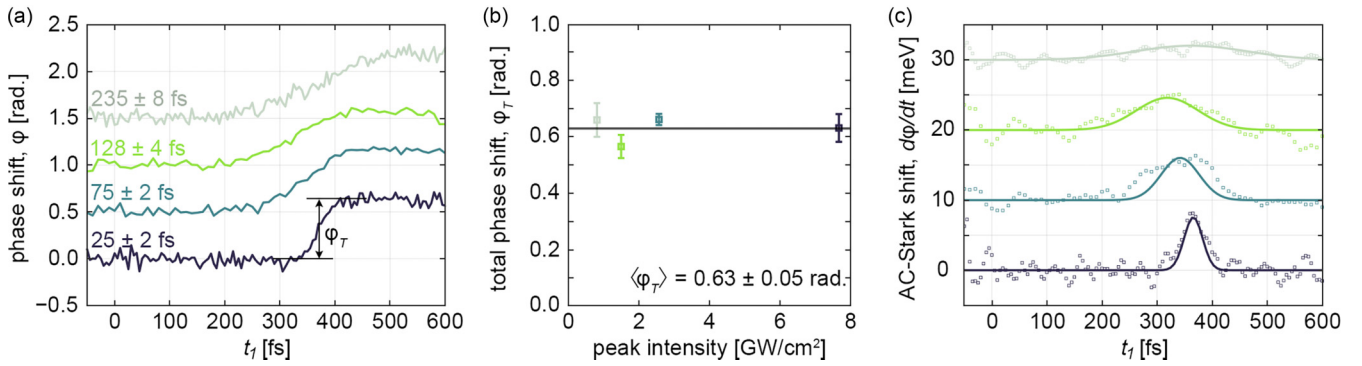
FIG. 4. (a) Signal phase dynamics integrated around the exciton energy as a function of t_1, for the four different pump pulses in Fig. 1(c) (offset vertically by 0.5 rad.). (b) The magnitude of the total phase shift, ϕ_T, is identical for each pump duration because the pump pulses have the same total fluence, consistent with the idealized Floquet formalism. We demonstrate a phase rotation of 0.63 ± 0.05 rad., extracted from a difference between the phase shift in (a) before and after the pump. (c) The derivative of the phase dynamics in (a) provides the instantaneous AC-Stark shift which responds as fast as the pulse envelope. Data is smoothed by an eight-point (80 fs) moving mean and fit by a Gaussian, with FWHM extracted from a cross correlation between the excitation pulse $\mathbf{k}_1^+$ and pump pulse (39, 81, 131, and 237 fs). The fit center and amplitude are free parameters. Each pump is offset vertically by 10 meV for clarity.

linearly proportional to the instantaneous pump intensity [20]. Taking the derivative of the phase shift with respect to t_1 gives the instantaneous blue shift, as shown in Fig. 4(c). A Gaussian fit of these data show that the measured blue-shift closely follows the cross-correlation of the $\mathbf{k}_1^+$ pulse and the pump pulse, even for the shortest pump pulse. From these plots we obtain a peak AC-Stark shift ranging between 2.0 and 7.5 meV for the longest and shortest pump pulse durations, respectively.

While the peak AC-Stark shift is controlled by the peak intensity, the total accumulated phase shift is determined by integrating the blue shift over the duration of the pump pulse. It is apparent then, that the total accumulated phase should be proportional to the pump fluence [4,5,13,14,17,18]. In the present measurements, where the fluence was kept constant, the accumulated phase shift should therefore be constant regardless of the pulse duration. By comparing the phase shift before and after the pump pulse [ϕ_T in Fig. 4(a)], we obtain an averaged total phase shift of 0.63 ± 0.05 rad., which remained constant as the pulse duration (peak intensity) was changed, as shown in Fig. 4(b). The magnitude of this shift is consistent with the fluence dependent phase shifts acquired in Ref. [20].

This phase response is representative of the idealized Floquet formalism, and is resolved despite the magnitude of the macroscopic coherence being reduced by more than 30% as a result of carrier induced scattering. In fact, from the phase dynamics observed here, there is no evidence of the two-photon absorption, nor any nonadiabaticity or inconsistency with Floquet theory. Additionally, our phase response is consistent with the phase response in Ref. [20], where no two-photon absorption was evident.

IV. CONCLUSIONS

The results presented here demonstrate the ability of MDCS to quantify changes to the bandstructure of monolayer WS$_2$ induced by Floquet engineering, even in the presence of significant broadening. This was achieved by following the

evolution of the average phase of the macroscopic coherence excited by the MDCS pulses. Furthermore, we were able to quantify the decoherence caused by carriers excited by two-photon absorption of the Floquet pump pulses, through the evolution of the signal amplitude. Being able to follow the evolution of the bandstructure, while at the same time quantifying the effect of excess carriers is an important step toward understanding the role of excited carriers in heating and driving nonadiabatic effects in Floquet engineering of solid state systems. Previous work has shown that scattering can prevent the formation of Floquet-Bloch bands when the scattering time is faster than the period of the driving field [12]. Even with the excess carriers, we are far from this regime, with driving period of 2.3 fs and scattering time in the hundreds of fs. Further, based on measurements of the exciton-exciton interaction strength in monolayer TMDCs [28], we expect that even with carrier densities beyond 10^{13} cm^{-2} the scattering time will remain longer than the drive period, which enhances the prospect that these excess carriers can be used to help shape the new potential energy environment and resultant band structures [10,11]. Finally, these measurements indicate that it should be possible to measure the effects of a Floquet-topological phase transition in monolayer TMDCs, even though a high density of carriers, excited by the above bandgap drive, are inevitable.

[1] J. H. Shirley, Solution of the Schrödinger equation with a Hamiltonian periodic in time, Phys. Rev. **138**, B979 (1965).

[2] Y. Wang, H. Steinberg, P. Jarillo-Herrero, and N. Gedik, Observation of Floquet-Bloch states on the surface of a topological insulator, Science **342**, 453 (2013).

[3] S. Zhou, C. Bao, B. Fan, F. Wang, H. Zhong, H. Zhang, P. Tang, W. Duan, and S. Zhou, Floquet engineering of black phosphorus upon below-gap pumping, Phys. Rev. Lett. **131**, 116401 (2023).

[4] J. Kim, X. Hong, C. Jin, S.-F. Shi, C.-Y. S. Chang, M.-H. Chiu, L.-J. Li, and F. Wang, Ultrafast generation of pseudo-magnetic field for valley excitons in WSe$_2$ monolayers, Science **346**, 1205 (2014).

[5] E. J. Sie, J. W. McIver, Y.-H. Lee, L. Fu, J. Kong, and N. Gedik, Valley-selective optical Stark effect in monolayer WS$_2$, Nat. Mater. **14**, 290 (2015).

[6] Y. Kobayashi, C. Heide, A. C. Johnson, V. Tiwari, F. Liu, D. A. Reis, T. F. Heinz, and S. Ghimire, Floquet engineering of strongly driven excitons in monolayer tungsten disulfide, Nat. Phys. **19**, 171 (2023).

[7] N. H. Lindner, G. Refael, and G. Victor, Floquet topological insulator in semiconductor quantum wells, Nat. Phys. **7**, 490 (2011).

[8] J. W. McIver, B. Schulte, F.-U. Stein, T. Matsuyama, G. Jotzu, G. Meier, and A. Cavalleri, Light-induced anomalous Hall effect in graphene, Nat. Phys. **16**, 38 (2020).

[9] M. Claassen, C. Jia, B. Moritz, and T. P. Devereaux, All-optical materials design of chiral edge modes in transition-metal dichalcogenides, Nat. Commun. **7**, 13074 (2016).

[10] K. I. Seetharam, C.-E. Bardyn, N. H. Lindner, M. S. Rudner, and G. Refael, Controlled population of Floquet-Bloch states via coupling to Bose and Fermi baths, Phys. Rev. X **5**, 041050 (2015).

[11] M. S. Rudner and N. H. Lindner, Band structure engineering and non-equilibrium dynamics in Floquet topological insulators, Nat. Rev. Phys. **2**, 229 (2020).

[12] S. Aeschlimann, S. A. Sato, R. Krause, M. Chávez-Cervantes, U. De Giovannini, H. Hübener, S. Forti, C. Coletti, K. Hanff, K. Rossnagel *et al.*, Survival of Floquet-Bloch states in the presence of scattering, Nano Lett. **21**, 5028 (2021).

[13] E. J. Sie, C. H. Lui, Y.-H. Lee, L. Fu, J. Kong, and N. Gedik, Large, valley-exclusive Bloch-Siegert shift in monolayer WS$_2$, Science **355**, 1066 (2017).

[14] Z. Ye, D. Sun, and T. F. Heinz, Optical manipulation of valley pseudospin, Nat. Phys. **13**, 26 (2017).

[15] T. LaMountain, H. Bergeron, I. Balla, T. K. Stanev, M. C. Hersam, and N. P. Stern, Valley-selective optical Stark effect probed by Kerr rotation, Phys. Rev. B **97**, 045307 (2018).

[16] C.-K. Yong, J. Horng, Y. Shen, H. Cai, A. Wang, C.-S. Yang, C.-K. Lin, S. Zhao, K. Watanabe, T. Taniguchi *et al.*, Biexcitonic optical Stark effects in monolayer molybdenum diselenide, Nat. Phys. **14**, 1092 (2018).

[17] P. D. Cunningham, A. T. Hanbicki, T. L. Reinecke, K. M. McCreary, and B. T. Jonker, Resonant optical Stark effect in monolayer WS$_2$, Nat. Commun. **10**, 5539 (2019).

[18] D. J. Morrow, D. D. Kohler, Y. Zhao, J. M. Scheeler, S. Jin, and J. C. Wright, Quantum interference between the optical Stark effect and resonant harmonic generation in WS$_2$, Phys. Rev. B **102**, 161401(R) (2020).

[19] S. K. Earl, M. A. Conway, J. B. Muir, M. Wurdack, E. A. Ostrovskaya, J. O. Tollerud, and J. A. Davis, Coherent dynamics of Floquet-Bloch states in monolayer WS$_2$ reveals fast adiabatic switching, Phys. Rev. B **104**, L060303 (2021).

[20] M. A. Conway, S. K. Earl, J. B. Muir, T.-H.-Y. Vu, J. O. Tollerud, K. Watanabe, T. Taniguchi, M. S. Fuhrer, M. T. Edmonds, and J. A. Davis, Effects of Floquet engineering on the coherent exciton dynamics in monolayer WS$_2$, ACS Nano **17**, 14545 (2023).

[21] S. A. Sato, J. W. McIver, M. Nuske, P. Tang, G. Jotzu, B. Schulte, H. Hübener, U. De Giovannini, L. Mathey, M. A. Sentef, A. Cavalleri, and A. Rubio, Microscopic theory for the light-induced anomalous Hall effect in graphene, Phys. Rev. B **99**, 214302 (2019).

[22] J. O. Tollerud and J. A. Davis, Coherent multi-dimensional spectroscopy: Experimental considerations, direct comparisons and new capabilities, Prog. Quantum Electron. **55**, 1 (2017).

[23] J. B. Muir, J. Levinsen, S. K. Earl, M. A. Conway, J. H. Cole, M. Wurdack, R. Mishra, J. David, E. Estrecho, Y. Lu *et al.*, Interactions between Fermi polarons in monolayer WS$_2$, Nat. Commun. **13**, 6164 (2022).

[24] K. Hao, L. Xu, P. Nagler, A. Singh, K. Tran, C. K. Dass, C. Schüller, T. Korn, X. Li, and G. Moody, Coherent and incoherent coupling dynamics between neutral and charged excitons in monolayer MoSe$_2$, Nano Lett. **16**, 5109 (2016).

[25] See Supplemental Material at http://link.aps.org/supplemental/10.1103/PhysRevB.109.104302 for details of sample preparation and characterization, spectra for the pump and MDCS pulses, homogeneous linewidth dependence on exciton density, and fitting of the photon echo response.

[26] J. C. Vaughan, T. Hornung, T. Feurer, and K. A. Nelson, Diffraction-based femtosecond pulse shaping with a two-dimensional spatial light modulator, Opt. Lett. **30**, 323 (2005).

[27] B. Xu, J. M. Gunn, J. M. D. Cruz, V. V. Lozovoy, and M. Dantus, Quantitative investigation of the multiphoton intrapulse interference phase scan method for simultaneous phase measurement and compensation of femtosecond laser pulses, J. Opt. Soc. Am. B **23**, 750 (2006).

[28] G. Moody, C. Kavir Dass, K. Hao, C.-H. Chen, L.-J. Li, A. Singh, K. Tran, G. Clark, X. Xu, G. Berghäuser *et al.*, Intrinsic homogeneous linewidth and broadening mechanisms of excitons in monolayer transition metal dichalcogenides, Nat. Commun. **6**, 8315 (2015).

[29] M. E. Siemens, G. Moody, H. Li, A. D. Bristow, and S. T. Cundiff, Resonance lineshapes in two-dimensional Fourier transform spectroscopy, Opt. Express **18**, 17699 (2010).

[30] J. D. Bell, R. Conrad, and M. E. Siemens, Analytical calculation of two-dimensional spectra, Opt. Lett. **40**, 1157 (2015).

[31] W. Wang, N. Sui, Z. Kang, Q. Zhou, L. Li, X. Chi, H. Zhang, X. He, B. Zhao, and Y. Wang, Cooling and diffusion characteristics of a hot carrier in the monolayer WS$_2$, Opt. Express **29**, 7736 (2021).

[32] S. Sim, J. Park, J.-G. Song, C. In, Y.-S. Lee, H. Kim, and H. Choi, Exciton dynamics in atomically thin MoS$_2$: interexcitonic interaction and broadening kinetics, Phys. Rev. B **88**, 075434 (2013).

[33] T. Korn, S. Heydrich, M. Hirmer, J. Schmutzler, and C. Schüller, Low-temperature photocarrier dynamics in monolayer MoS$_2$, Appl. Phys. Lett. **99**, 102109 (2011).

[34] Q. Wang, S. Ge, X. Li, J. Qiu, Y. Ji, J. Feng, and D. Sun, Valley carrier dynamics in monolayer molybdenum disulfide

from helicity-resolved ultrafast pump-probe spectroscopy, ACS Nano **7**, 11087 (2013).

[35] H. Shi, R. Yan, S. Bertolazzi, J. Brivio, B. Gao, A. Kis, D. Jena, H. G. Xing, and L. Huang, Exciton dynamics in suspended monolayer and few-layer MoS_2 2D crystals, ACS Nano **7**, 1072 (2013).

[36] J. Gao, B. Li, J. Tan, P. Chow, T.-M. Lu, and N. Koratkar, Aging of transition metal dichalcogenide monolayers, ACS Nano **10**, 2628 (2016).

[37] J. C. Kotsakidis, Q. Zhang, A. L. Vazquez de Parga, M. Currie, K. Helmerson, D. K. Gaskill, and M. S. Fuhrer, Oxidation of monolayer WS_2 in ambient is a photoinduced process, Nano Lett. **19**, 5205 (2019).

[38] P. V. Kolesnichenko, Q. Zhang, T. Yun, C. Zheng, M. S. Fuhrer, and J. A. Davis, Disentangling the effects of doping, strain and disorder in monolayer WS_2 by optical spectroscopy, 2D Mater. **7**, 025008 (2020).